

OPTIMIZATION OF DOPING PROCESS TOWARDS RUTILE-PHASED
TITANIUM DIOXIDE NANORODS ARRAY FOR ULTRAVIOLET
PHOTODETECTOR APPLICATIONS

SALINA BINTI MOHAMMAD MOKHTAR

A thesis submitted in
fulfilment of the requirement for the award of the
Doctor of Philosophy in Electrical Engineering

Faculty of Electrical and Electronic Engineering
Universiti Tun Hussein Onn Malaysia

AUGUST 2023

DEDICATION

This thesis was dedicated to my parents; Mohammad Mokhtar bin Mohammad,
Rabiah binti Ibrahim,
and my husband; Mohamad Najib bin Kammalluden



ACKNOWLEDGEMENT

First and foremost, I would like to express my highest gratitude to my research supervisor, Assoc. Prof. Dr Mohd Khairul bin Ahmad for his guidance and encouragement throughout the research period. My thesis would not have been possible without his excellent supervision, support, and guidance. I would like to express my sincere appreciation to Prof. Masaru Shimomura for giving me the opportunity to continue my study at Shizuoka University, and also for his advice and support for this research.

Special thanks given to all members of Microelectronics & Nanotechnology–Shamsuddin Research Centre (MiNT-SRC) that were present throughout my journey for their help and support to complete my research. I would also like to thank all the staff members of the Graduate School of Science and Technology, and Nano Device Centre at Shizuoka University for their kind support and patience.

Finally, I would like to express my deepest thanks to my husband, Mohamad Najib for his love, encouragement, understanding, and full support during my entire research period. Thank you for being there for me. To my mother, Rabiah, thank you for all the advices that have been given and thank you for being there. My sisters and brothers, you all have been nothing but supportive siblings to me during these times. Special thanks to my parents and sister-in-law for their love and encouragement. Last but not least, to my abah, again this is for you. I love you.

ABSTRACT

Titanium dioxide has gained attention in current fundamental research for photodetector application. Commercial UV photodetectors use Si-based materials that have a low bandgap and need a filter to filter-out visible light wavelengths. For that reason, TiO₂ is widely studied as it has a wide bandgap that absorbs only UV wavelength. Even so, the slow carrier transport of TiO₂ has been considered a drawback that can limit its full potential in these applications. Focusing on the electronic properties of the material, this study used several dopant concentrations to enhance rutile TiO₂ electron concentration and mobility by using niobium (Nb) and boron (B) as dopants in nanorods TiO₂. Well-aligned TiO₂ nanorods were fabricated with 1.00 mL of TiO₂ precursor as a preliminary study. Herein, the Nb and B-doped rutile TiO₂ nanorods were fabricated by using hydrothermal method with FTO as a substrate. Based on the finding, doping process was successfully done with confirmation on the presence of Nb and B dopants in TiO₂ lattice by XPS spectroscopy. Photocurrent analysis of the TiO₂ nanorods shows increasing current approximately 2.3 times larger than undoped TiO₂ for 0.25 w.t.% Nb doped, and 1.8 times larger for 1.00 w.t.% of B doped with bandgap of 3.09 and 3.04 eV, respectively. While B doping does not give significant changes to the nanorod, Nb dopant inhibits nucleation sites on the FTO thus reducing the density of nanorods in high doping concentration. Annealing treatment was done to enhance the crystallinity of the nanorods with the annealing temperature varied from 200 to 500 °C. Annealing treatment on both samples showed an increase in the photocurrent with enhancement on the crystallinity of samples at 300 °C annealing temperature. The results prove that electron concentration and mobility of rutile TiO₂ nanorods can be enhanced by using Nb and B dopants. Highly crystalline nanorods can be achieved with annealing treatment at 300 °C that will further enhance the electronic properties of rutile TiO₂ nanorods thus making it beneficial in UV photodetector application.

ABSTRAK

Titanium dioksida telah mendapat perhatian dalam penyelidikan asas untuk aplikasi pengesan foto. Pengesan foto UV komersial menggunakan bahan berasaskan Si yang mempunyai jurang jalur yang rendah dan memerlukan penapis untuk menapis jarak gelombang cahaya yang boleh dilihat. Atas sebab itu, TiO₂ dikaji secara meluas kerana ia mempunyai jurang jalur lebar yang hanya menyerap jarak gelombang UV. Walaupun begitu, pengangkutan pembawa TiO₂ yang perlahan telah dianggap sebagai kelemahan yang boleh mengehadkan potensi penuhnya dalam aplikasi ini. Memfokuskan kepada sifat elektronik bahan, kajian ini menggunakan beberapa kepekatan dopan untuk meningkatkan kepekatan dan mobiliti elektron TiO₂ rutil dengan menggunakan niobium (Nb) dan boron (B) sebagai dopan dalam nanorod TiO₂. Nanorod TiO₂ yang jajar telah dibuat dengan 1.00 mL prekursor TiO₂. Di sini, nanorod TiO₂ rutil terdop Nb dan B telah dibuat dengan menggunakan kaedah hidroterma dengan FTO sebagai substrat. Berdasarkan penemuan, proses doping telah berjaya dilakukan dengan pengesanan kehadiran Nb dan B dopan dalam kekisi TiO₂ oleh spektroskopi XPS. Analisis arus foto bagi nanorod TiO₂ menunjukkan peningkatan arus kira-kira 2.3 kali lebih besar daripada TiO₂ yang tidak didop dengan nilai 0.25 w.t.% oleh dopan Nb, dan 1.8 kali lebih besar dengan nilai 1.00 w.t.% oleh dopan B. Walaupun doping B tidak memberikan perubahan ketara kepada morfologi nanorod, dopan Nb telah menghalang tapak nukleasi diatas FTO sekali gus mengurangkan ketumpatan nanorod dalam kepekatan doping yang tinggi. Rawatan penyepuhlindapan telah dilakukan untuk meningkatkan kehabluran nanorod dengan suhu penyepuhlindapan yang berbeza-beza dari 200 hingga 500 °C. Rawatan penyepuhlindapan pada kedua-dua sampel menunjukkan peningkatan dalam arus foto dan pada kehabluran sampel dengan suhu penyepuhlindapan 300 °C. Ini menunjukkan bahawa kepekatan elektron dan mobiliti nanorod TiO₂ rutil boleh dipertingkatkan dengan menggunakan dopan Nb dan B.

CONTENTS

	TITLE	i
	DECLARATION	ii
	DEDICATION	iii
	ACKNOWLEDGEMENT	vii
	ABSTRACT	v
	ABSTRAK	vi
	CONTENTS	vii
	LIST OF TABLES	ix
	LIST OF FIGURES	x
	LIST OF SYMBOLS AND ABBREVIATION	xi
	LIST OF APPENDICES	xii
CHAPTER 1	INTRODUCTION	1
	1.1 Background study	1
	1.2 Problem statement	5
	1.3 Objective of the research	6
	1.4 Research scope	7
	1.5 Research contribution	7
	1.6 Summary	8
CHAPTER 2	LITERATURE REVIEW	9
	2.1 Introduction	9
	2.2 Development methods of titanium dioxide nanostructure	10
	2.2.1 Spray pyrolysis deposition method	10
	2.2.2 Chemical vapor deposition	11

2.2.3	Sol-gel methods	12
2.2.4	Ultrasonic-assisted methods	13
2.2.5	Others	14
2.3	Fabrication titanium dioxide nanorods array using hydrothermal method	16
2.4	Development of ultraviolet photoconductive sensor using titanium dioxide nanomaterials	18
2.5	Doping of Titanium Dioxide	21
2.5.1	Fabrication of Niobium-doped Titanium Dioxide Nanomaterials	24
2.5.2	Fabrication of Boron-doped Titanium Dioxide Nanomaterials	26
2.6	Summary	27
CHAPTER 3 THEORY AND METHODOLOGY		29
3.1	An overview of research methodology	29
3.2	Substrate cleaning	29
3.3	Preparation of undoped titanium dioxide nanorods arrays via hydrothermal reaction method	31
3.4	Preparation of doped titanium dioxide nanorods arrays via hydrothermal reaction method	35
3.4.1	Nb-doped rutile TiO ₂ nanorods	35
3.4.2	Annealed Nb-doped rutile TiO ₂ nanorods	36
3.4.3	B-doped rutile TiO ₂ nanorods	37
3.4.4	Annealed B-doped TiO ₂ nanorods	38
3.5	Titanium Dioxide Nanostructured Thin Film Characterization Methods	39
3.5.1	Structural analysis	39
3.5.2	Morphological analysis	42
3.5.3	Optical analysis	44
3.6	Photodetection analysis for titanium dioxide-based ultraviolet photodetector	45
3.7	Summary	47
CHAPTER 4 RESULTS AND DISCUSSION		48
4.1	Preliminary study and fabrication of undoped rutile titanium dioxide nanorods	48
4.1.1	Comparison of FTO substrate from different manufacturers	48
4.1.2	Early growth of titanium dioxide nanorods arrays on FTO substrate	50

4.1.3	Effect of different amounts of precursor on the fabrication of TiO ₂ nanorods	51
4.1.4	Summary	54
4.2	Fabrication of Nb-doped titanium dioxide nanorods arrays with different percentages of Nb ⁵⁺ dopant	56
4.2.1	Analysis on morphological properties of Nb-doped titanium dioxide nanorods	56
4.2.2	Analysis on optical and photodetector properties of Nb-doped TiO ₂ nanorods	68
4.2.3	Effect of Nb-doped rutile TiO ₂ nanorods on photodetector properties	70
4.2.4	Summary	72
4.3	Fabrication of annealed Nb-doped titanium dioxide nanorods arrays with different annealing temperature	73
4.3.1	Analysis on morphological properties of annealed Nb-doped titanium dioxide nanorods	73
4.3.2	Analysis on optical and photodetector properties of annealed Nb-doped TiO ₂ nanorods	82
4.3.3	Effect of annealed Nb-doped rutile TiO ₂ nanorods on photodetector properties	84
4.3.4	Summary	86
4.4	Fabrication of B-doped titanium dioxide nanorods arrays with different percentage of B ³⁻ dopant	86
4.4.1	Analysis on morphological properties of B-doped titanium dioxide nanorods	87
4.4.2	Analysis on optical and photodetector properties of B-doped TiO ₂ nanorods	92
4.4.3	Effect of B-doped rutile TiO ₂ nanorods on photodetector properties	97
4.4.4	Summary	98
4.5	Fabrication of annealed B-doped titanium dioxide nanorods arrays with different annealing temperatures	99
4.5.1	Analysis on morphological properties of annealed B-doped titanium dioxide nanorods	99

4.5.2	Analysis on optical and photodetector properties of annealed B-doped TiO ₂ nanorods	104
4.5.3	Summary	105
4.6	Optimization summary of Nb and B doped titanium dioxide and its annealing treatment	105
CHAPTER 5	CONCLUSION AND FUTURE WORKS	108
5.1	Conclusions	108
5.2	Recommendations	111
	REFERENCES	112
	APPENDICES	127



LIST OF TABLES

2.1	Fabrication methods used to fabricate a titanium dioxide nanorods/nanostructure	15
3.1	Preparation of TiO ₂ solution, fabrication process, and characterization technique for optimization of TiO ₂ nanorods using different amounts of precursor	34
3.2	Preparation of Nb-doped TiO ₂ solution, fabrication process, and characterization technique for optimization of TiO ₂ nanorods doped with different Nb weight percentage	36
3.3	Preparation of annealed Nb-doped TiO ₂ solution, fabrication process, and characterization technique on samples with different annealing temperatures	37
3.4	Preparation of B-doped TiO ₂ solution, fabrication process, and characterization technique for optimization of TiO ₂ nanorods doped with different B weight percentage	38
3.5	Preparation of annealed B-doped TiO ₂ solution, fabrication process, and characterization technique on samples with different annealing temperatures	38
4.1	Surface roughness, Ra of FTO substrates from Sigma Aldrich and SPD Laboratory	49
4.2	FWHM, crystallite size, and Raman percentage of Nb-doped TiO ₂ nanorods arrays	57
4.3	Elemental ratio (Nb/Ti) of Nb-doped TiO ₂ nanorods arrays calculated from XPS spectra	63
4.4	Photocurrent values of Nb-doped TiO ₂ nanorods arrays	

4.5	Crystallite size and Raman ratio of as-prepared and annealed Nb-doped rutile TiO ₂ nanorods arrays at 200, 300, 400, and 500 °C	
4.6	Elemental ratio (Nb/Ti) of annealed Nb-doped rutile TiO ₂ nanorods arrays from XPS spectra	78
4.7	Surface area calculated for as-prepared and annealed Nb-doped TiO ₂ nanorods	80
4.8	Photocurrent values of annealed Nb-doped rutile TiO ₂ nanorods arrays	84
4.9	FWHM, crystallite size, and Raman percentage of B-doped rutile TiO ₂ nanorods arrays	88
4.10	Photocurrent values of undoped and 0.25, 0.50, and 1.00 w.t.% B-doped rutile TiO ₂ nanorods arrays	98
4.11	Crystallite size and Raman ratio of as-prepared and annealed B-doped rutile TiO ₂ nanorods arrays	100
4.12	Photocurrent values of annealed B-doped rutile TiO ₂ nanorods arrays	105
4.13	Photocurrent value of Nb and B dopant from different dopant concentration	106
4.14	Photocurrent value of Nb and B doped TiO ₂ nanorods from different annealing temperature	107

LIST OF FIGURES

1.1	Electromagnetic spectrum showing the wavelength of three types of ultraviolet that is UVA, UVB, and UVC	2
1.2	The schematic conventional unit cells for (a) anatase, (b) rutile, and (c) brookite TiO ₂ [6]	2
1.3	TiO ₂ morphology in (a) nanorods, (b) nanoflowers, and (c) nanotubes [12], [13], [16]	3
2.1	Schematic diagram of spray pyrolysis deposition method [44]	11
2.2	Schematic diagram of chemical vapor deposition fabrication process	11
2.3	Schematic diagrams of sol-gel process and its final products with different drying process [52]	13
2.4	Schematic diagram of example of ultrasonication cavitation effects [55]	14
2.5	TiO ₂ nanorods with branches synthesized from immersing the nanorods into TiCl ₄ solution for (a) 6, (b) 12, (c) 18, and (d) 24 hours with its IPCE analysis [81]	20
2.6	SEM image of TiO ₂ nanowires fabricated on (a) ITO substrate, (b) FTO substrate and (c) I–V characteristics of the devices in dark and under 350 nm UV light illumination (Insets show the device structure and schematic illustration of the back-to-back Schottky junctions) [83]	21
2.7	Illustration of a host material being doped with (a) n-type doping with extra electrons from impurities and (b) p-type doping with vacancies	22
2.8	Titanium dioxide bandgap with undoped lattice at $h\nu_1$, metal-doped TiO ₂ at $h\nu_2$, and non-metal doped TiO ₂ at $h\nu_3$ [84]	23
3.1	Flowchart of the experiment's process	30

3.2	Steps of substrate cleaning process	31
3.3	Schematic illustration of the fabrication route of undoped rutile TiO ₂ nanorods	33
3.4	The illustration of steel-made autoclave used for the hydrothermal reaction	33
3.5	Summarized steps to fabricate titanium dioxide nanorods array using the hydrothermal reaction method	34
3.6	Schematic illustration of the fabrication route of Nb and B doped rutile TiO ₂ nanorods	35
3.7	Schematic diagram of typical X-ray diffraction system	40
3.8	Schematic diagram of typical Raman spectroscopy system	41
3.9	Schematic diagram of X-ray photoelectron spectroscopy	42
3.10	Schematic diagram of field-emission scanning electron microscopy sample stage	43
3.11	Schematic diagram of transmission electron microscopy	44
3.12	Schematic diagram of UV-vis-NIR spectroscopy	45
3.13	Schematic diagram of self-powered UV photodetector with DSSC-like structure (without dye) based on photo-electrochemical cells	47
4.1	Figure 4.1: AFM images of FTO films from (a) Sigma Aldrich and (b) SPD Laboratory ⁵²	49
4.2	FESEM images of FTO substrate from (a) Sigma Aldrich and (b) SPD Laboratory	50
4.3	FESEM images of the early growth of TiO ₂ nanorods in comparison with (a) bare FTO substrate with hydrothermal fabrication time of (a) 90, (b) 120, (c) 210, and (d) 225 min	51
4.4	X-ray diffraction patterns of TiO ₂ nanorods fabricated with (a) 0.50, (b) 0.75, (c) 1.00, and (d) 1.50 mL of TBOT precursor	52
4.5	Raman spectra of TiO ₂ nanorods fabricated with (a) 0.50, (b) 0.75, (b) 1.00, and (d) 1.50 mL of TBOT precursor	53

4.6	FESEM images from the top view of (a) 0.50, (b) 0.75, (c) 1.00, and (d) 1.50 mL of TBOT with the cross-sectional view of (a1) 0.50, (b1) 0.75, (c1) 1.00, and (d1) 1.50 mL of TBOT	55
4.7	X-ray diffraction patterns of (a) FTO substrate and TiO ₂ nanorods fabricated with (b) undoped, (c) 0.25, (d) 0.50, and (e) 1.00 w.t.% of Nb dopant	57
4.8	Possible doping structure of TiO ₂ lattice after doping with Nb atom substituting Ti atom [115]	58
4.9	Raman spectroscopy of TiO ₂ nanorods fabricated with (a) undoped, (b) 0.25, (c) 0.50, and (d) 1.00 w.t.% of Nb dopant	59
4.10	Wide XPS spectroscopy of undoped and Nb-doped TiO ₂ nanorods arrays with Ti, O, and C element detected from 0.00 to 0.50 w.t. % and additional of Sn element for 1.00 w.t.%	60
4.11	Narrow XPS spectroscopy of Ti 2p obtained from (a) undoped, (b) 0.25, (c) 0.50, (d) 1.00 and Nb 3d of (e) undoped, (f) 0.25, (g) 0.50, (h) 1.00 w.t.% Nb dopant concentration	61
4.12	Narrow XPS spectroscopy of O 1s obtained from (a) undoped, (b) 0.25, (c) 0.50, and (d) 1.00 w.t.% Nb-doped TiO ₂ nanorods arrays	62
4.13	FESEM images from the top view of (a) 0.00, (b) 0.25, (c) 0.50, and (d) 1.00 w.t.% of Nb dopant with the cross-sectional view of (e) 0.00, (f) 0.25, (g) 0.50, and (h) 1.00 w.t.% of Nb dopant	64
4.14	TEM images of (a) 0.00, (b) 0.25, (c) 0.50, and (d) 1.00 w.t.% of Nb dopant with its corresponding HRTEM images (a1) 0.00, (b1) 0.25, (c1) 0.50, and (d1) 1.00 w.t.% of Nb dopant	65
4.15	Magnified HRTEM images of 0.50 w.t.% Nb-doped TiO ₂ nanorods arrays	65
4.16	Growth mechanism of Nb-doped rutile TiO ₂ nanorods	66
4.17	Morphological images of (a) TiO ₂ nanorods seed layer after 3h hydrothermal reaction, and (b) TiO ₂ nanorods after 13h hydrothermal reaction with 1.00 w.t.% of Nb	67
4.18	XPS of (a) wide and (b) core-level spectra of FTO substrate with Nb attached on the surface	67
4.19	Morphological images of (a) FTO substrate with Nb attached on the surface, and (b) TiO ₂ nanorods fabricated on FTO with Nb attached on the surface	68

4.20	Reflectance spectra of (a) undoped, (b) 0.25, (c) 0.50, and (d) 1.00 w.t.% Nb-doped TiO ₂ nanorods	69
4.21	Bandgap energy of (a) undoped, (b) 0.25, (c) 0.50, and (d) 1.00 w.t.% Nb-doped TiO ₂ nanorods calculated with Kubelka Munk's equation	69
4.22	Schematic diagram of self-powered UV photodetector with DSSC-like structure (without dye) based on photo-electrochemical cells	70
4.23	Photocurrent characteristics of undoped, 0.25, 0.50, and 1.00 w.t.% Nb-doped TiO ₂ nanorod arrays measured under alternating on/off UV lamp states	71
4.24	Nyquist plot of undoped, 0.25, 0.50, and 1.00 w.t.% Nb-doped TiO ₂ nanorod arrays	72
4.25	X-ray diffraction spectra of (a) as-prepared and annealed Nb-doped TiO ₂ nanorod arrays at (b) 200, (c) 300, (d) 400, and (e) 500 °C	74
4.26	Raman spectroscopy of (a) as-prepared and annealed Nb-doped rutile TiO ₂ nanorod arrays at (b) 200, (c) 300, (d) 400, and (e) 500 °C	75
4.27	Wide XPS spectroscopy of as-prepared and annealed Nb-doped rutile TiO ₂ nanorods arrays at 200, 300, 400, and 500 °C	77
4.28	Narrow XPS spectroscopy of Nb 3d from (a) as-prepared and annealed Nb-doped TiO ₂ nanorods arrays at (b) 200, (c) 300, (d) 400, and (e) 500 °C	77
4.29	Narrow XPS spectroscopy of Ti 2p obtained from (a) as-prepared, (b) 200 °C, (c) 300 °C, (d) 400 °C (e) 500 °C and Nb 3d obtained from (f) as-prepared, (g) 200 °C, (h) 300 °C (i) 400 °C and (j) 500 °C annealing temperature	79
4.30	FESEM images from the top view of (a) as-prepared and Nb-doped TiO ₂ annealed in (b) 200 °C, (c) 300 °C, (d) 400 °C (e) 500 °C annealing temperature and cross-sectional view of (f) as-prepared and Nb-doped TiO ₂ annealed in (g) 200 °C, (h) 300 °C (i) 400 °C and (j) 500 °C annealing temperature	81
4.31	TEM images of (a) as-prepared, (b) 300 °C (c) 500 °C and with its corresponding HRTEM images of (a) as-prepared, (b) 300 °C (c) 500 °C annealed Nb-doped TiO ₂ nanorods arrays. (d) Schematic diagram of the TiO ₂ nanorods before and after annealing treatment at 500 °C	82

4.32	Reflectance spectra of as-prepared and annealed Nb-doped TiO ₂ nanorod arrays at 200, 300, 400 and 500 °C	83
4.33	Kubelka Munk's plot of (a) as-prepared and annealed Nb-doped TiO ₂ nanorod arrays at (b) 200, (c) 300, (d) 400 and (e) 500 °C	83
4.34	Photocurrent response of as-prepared and annealed Nb-doped TiO ₂ nanorods arrays at 200, 300, 400 and 500 °C	85
4.35	Nyquist plot of as-prepared and annealed Nb-doped TiO ₂ nanorod arrays at 200, 300, 400 and 500 °C	85
4.36	X-ray diffraction patterns of TiO ₂ nanorods fabricated with (a) undoped, (b) 0.25, (c) 0.50, and (d) 1.00 w.t.% of B dopant	88
4.37	Possible doped structure of TiO ₂ lattice after doping with B atom substituting O atom [137]	89
4.38	Raman spectroscopy of rutile TiO ₂ nanorods TiO ₂ nanorods fabricated with (a) undoped, (b) 0.25, (c) 0.50, and (d) 1.00 w.t.% of B dopant	90
4.39	Wide XPS spectroscopy of undoped and 0.25, 0.50, 1.00 w.t.% B-doped rutile TiO ₂ nanorods arrays with Ti, O, and C element detected	91
4.40	Narrow XPS spectroscopy of Ti 2p from (a) undoped, (b) 0.25, (c) 0.50, (d) 1.00 w.t.% of B dopant and B 1s obtained from (f) undoped, (g) 0.25, (h) 0.50, (i) 1.00 w.t.% of B-doped TiO ₂ nanorods array	92
4.41	Narrow XPS spectroscopy of O 1s obtained from (a) undoped, (b) 0.25, (c) 0.50, and (d) 1.00 w.t.% of B-doped TiO ₂ nanorods array	93
4.42	FESEM images from the top view of (a) undoped, (b) 0.25, (c) 0.50, and (d) 1.00 w.t.% of B dopant with the cross-sectional view of (e) undoped, (f) 0.25, (g) 0.50, and (h) 1.00 w.t.% of B dopant	94
4.43	TEM images of B-doped TiO ₂ nanorods with (a) undoped, (b) 0.50, and (c) 1.00 w.t.% of dopant and its corresponding HRTEM (a1) undoped, (b1) 0.25, and (c1) 1.00 w.t.% of B dopant	95
4.44	Absorbance spectra of undoped, 0.25, 0.50. and 1.00 w.t.% of B-doped rutile TiO ₂ nanorods	96
4.45	Bandgap energy of undoped and 0.25, 0.50. and 1.00 w.t.% B-doped rutile TiO ₂ nanorods calculated with Tauc's plot equation	96

4.46	Photocurrent response of undoped and 0.25, 0.50. and 1.00 w.t.% B-doped rutile TiO ₂ nanorods arrays.	97
4.47	Nyquist plot of undoped and 0.25, 0.50. and 1.00 w.t.% B-doped rutile TiO ₂ nanorods arrays	98
4.48	X-ray diffraction of (a) as-prepared B-doped rutile TiO ₂ nanorods and post-annealing treatment at (b) 200, (c) 300, (d) 400 and (d) 500 °C annealing temperature	100
4.49	Raman spectroscopy of (a) as-prepared B-doped rutile TiO ₂ nanorods and post-annealing treatment at (b) 200, (c) 300, (d) 400 and (d) 500 °C annealing temperature	101
4.50	FESEM images from the top view of (a) as-prepared, (b) 200 (c) 300, (d) 400, and (e) 500 °C post-annealing treatment with the cross-sectional view of (a1) as-prepared, (b1) 200 (c1) 300, (d1) 400, and (e1) 500 °C post-annealing treatment	103
4.51	Photocurrent of as-prepared and annealed B-doped rutile TiO ₂ nanorods at 200, 300, 400 and 500°C annealing temperature	104
4.52	Comparison of amount of photocurrent collected from different dopant concentration of Nb and B	106
4.53	Comparison of amount of photocurrent collected from different annealing temperature of Nb and B doped TiO ₂ nanorods	107



LIST OF SYMBOLS AND ABBREVIATIONS

°C	-	Degree Celsius
B	-	Boron
C	-	Carbon
CBD	-	Chemical bath deposition
CBM	-	Conduction band minimum
CVD	-	Chemical vapour deposition
D	-	Crystallite size
DI water	-	Deionized water
Eg	-	Bandgap
EIS	-	Electrochemical impedance spectroscopy
EtOH	-	Ethanol
FESEM	-	Field emission scanning electron microscopy
FTO	-	Fluorine-doped tin oxide
FWHM	-	Full-width half-maximum
GaN	-	Gallium nitrite
H ₂ O	-	Water
HCl	-	Hydrochloric acid
ITO	-	Indium-doped tin oxide
J _{sc}	-	Photocurrent
KCl	-	Potassium chloride
LiCl	-	Lithium chloride
Mg	-	Magnesium
μm	-	Micrometre
N	-	Nitrogen
NaCl	-	Sodium chloride
Nb	-	Niobium
nm	-	Nanometre

NPs	-	Nanoparticles
O	-	Oxygen
OH	-	Hydroxide
PEC	-	Photoelectrochemical
QDs	-	Quantum dots
SiC	-	Silicon carbide
Sn	-	Tin
TBOT	-	Titanium butoxide
TCO	-	Transparent conductive oxide
TEM	-	Transmission electron microscopy
TiO ₂	-	Titanium dioxide
Ti	-	Titanium
TiCl ₄	-	Titanium chloride
TTIP	-	Titanium isopropoxide
UV	-	Ultraviolet
w.t.%	-	Weight percentage
XPS	-	X-ray photoelectron spectroscopy
XRD	-	X-ray diffraction
ZnO	-	Zinc oxide



PTTA
PERPUSTAKAAN TUNJUKU AMINAH

LIST OF APPENDICES

APPENDIX	TITLE	PAGE
A	List of Publications	127
B	List of Awards	129
C	VITA	130



PTTA UTHM
PERPUSTAKAAN TUNKU TUN AMINAH

CHAPTER 1

INTRODUCTION

1.1 Background Study

Titanium dioxide (TiO_2) has emerged as a potential material in UV photoconductive sensor applications. Titanium dioxide has a direct and wide bandgap energy that allows it to strongly absorb UV light. When TiO_2 is illuminated with UV light, electrons from the valence band are excited into the conduction band to give rise to conductivity. The increase in conductivity due to the excitation of electrons under UV irradiation produces a signal that can be used for UV light detection. Photo-detection in the ultraviolet (UV) area has attracted attention due to its numerous applications in industries, instruments, and our daily life. Ultraviolet light is defined as a portion of the electromagnetic spectrum that also includes visible light, radio waves, X-rays and microwave, with wavelength ranging from 100 to 400 nm that can be further subdivided to: Vacuum UV (100-200 nm), UVC (200-280 nm), UVB (280-315 nm), and UVA (316-400 nm) [1]. It has wavelength that is shorter than visible light, but longer than X-rays as shown in Figure 1.1. With the focus being in the UVA, the direct bandgap of TiO_2 at 3.40 - 3.00 eV at room temperature [2], [3] is suitable as UVA energy lies in the range of 3.9 to 3.1 eV.

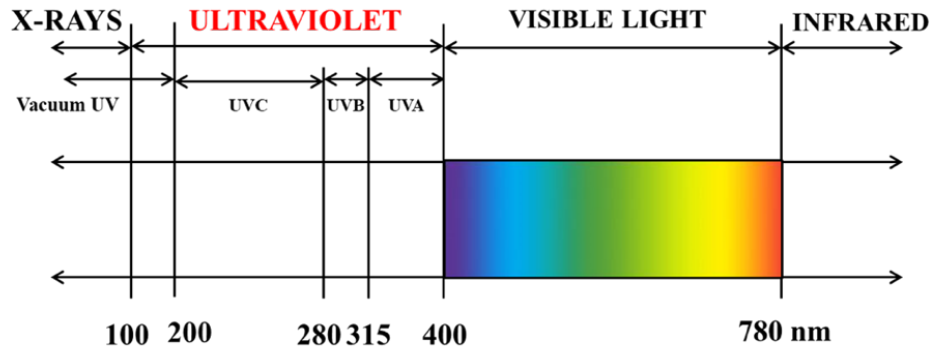


Figure 2.1: Electromagnetic spectrum showing the wavelength of three types of ultraviolet that is UVA, UVB, and UVC

TiO₂ has a melting point of 1825° which implies strong bonds and shows that it is a thermally and chemically resistant material [4]. Rutile, anatase, and brookite are three phases of TiO₂ that are widely known to have existed in either bulk structure or nanoparticles. Rutile has six atoms in a unit cell with each titanium atom is bonded to six oxygen atoms, meanwhile, each oxygen atom bonded to three titanium atoms. With a slightly more distorted structure compared to rutile, anatase structure has two of the titanium-oxygen bonds that are much longer than the other four bonds. On the other hand, brookite has the same interatomic distance to those of rutile and anatase, but different in its O-Ti-O bond angles [5]. Figure 1.2 shows the schematic conventional unit cells for (a) anatase, (b) rutile, and (c) brookite TiO₂. Each polymorph of titanium dioxide contributes to different uses. For rutile phased TiO₂, due to its high refractive index, it is usually used in high-grade, corrosion-protective white coatings and paint, or plastics, rubber, leather, and paper. The anatase phase has great pigment and optical properties due to its electronic structure and is usually used as an optical coating. Meanwhile, the application of brookite TiO₂ is restricted mainly because it was hard to be synthesized.

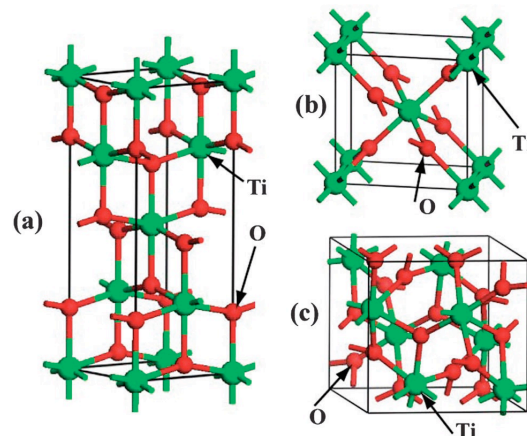


Figure 1.2: The schematic conventional unit cells for (a) anatase, (b) rutile, and (c) brookite TiO₂ [6]

Titanium dioxide is an important material because of its functional properties. For example, under certain conditions, it can absorb ultraviolet (UV) light, and is transparent to the visible light spectrum [7]. Additionally, TiO_2 is substantially less expensive than other materials and their reserve is abundant [8]. Its properties can also be altered chemically to enhance its properties, for example, through the doping process, which can provide free carriers to increase its efficiency as a photo-catalyst depending on the type of dopants used as different dopant may not have the same effect on trapping electrons and/or hole [9]. In nanomaterials, specific surface area and surface-to-volume ratio would increase as the size of nanomaterials decreases [10]. For TiO_2 -based devices, high surface area from small particle size would be advantageous. Thus, the performance of TiO_2 -based devices was primarily impacted by the sizes of TiO_2 materials itself, particularly at the nanometre scale.

Nanostructured materials have been extensively studied due to their potential use in fabricated micro and nanoscale devices. It has a very high aspect ratio, reduced power consumption, and higher integration densities than bulk materials. It also exhibits superior stability owing to its high crystallinity [11]. Titanium dioxide is a semiconductor material that can be shaped into various crystals. Nanowires, nanoflowers, nanorods, and nanofibers are among the many structures that have been reported in literatures as shown in Figure 1.3 [12]–[15]. Such structures exhibit novel properties that can facilitate the fabrication of novel and efficient nanoscale devices.

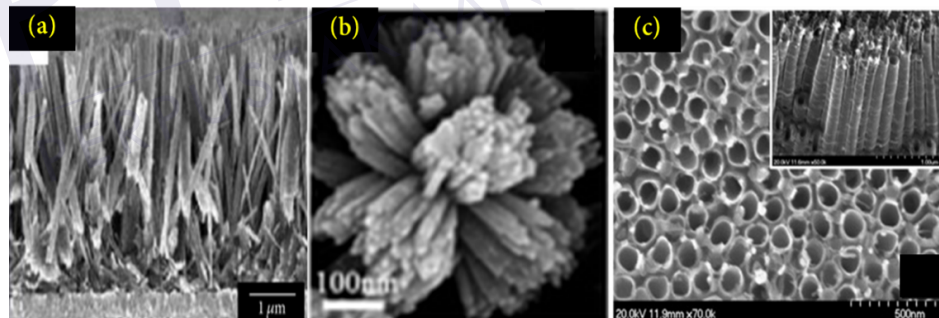


Figure 1.3: TiO_2 morphology in (a) nanorods, (b) nanoflowers, and (c) nanotubes [12], [13], [16]

Nanostructured TiO_2 has a large surface-to-volume ratio that can be used to enhance the performance of devices. As the size is reduced, devices become faster. This size reduction phenomenon also contributes to the quantum confinement phenomenon. Quantum confinement traps electrons in a small area in such a way that controlling the movement of the electrons in a particular direction becomes easier. Many investigations have focused on nanostructured TiO_2 for usage in fabricated devices, such as dye-sensitized solar cells, photocatalysts, various

sensors, and LEDs. Numerous structures of TiO₂ can be produced depending on the technique used. Example of the techniques include chemical bath deposition (CBD), hydrothermal method, sol-gel method, and RF sputtering. However, solution-based techniques are preferred in producing high-quality TiO₂ at a low cost and therefore allowing the fabrication of UV sensors at minimal cost. Furthermore, using this technique, the growth of TiO₂ structure can be easily controlled via the addition of a stabilizer or surfactant. The solution-based technique has additional advantages, such as facilitating the growth of TiO₂ at low temperatures at a large-scale with simple processing methods [17].

TiO₂ has been reported to be an intrinsically n-type semiconductor due to its oxygen deficiency [18], [19]. The intrinsic n-type conductivity of TiO₂ can be enhanced by introducing elements such as boron (B), nitrogen (N), niobium (Nb), and magnesium (Mg) [20]–[22]. The doping process is done to modify an intrinsic semiconductor in order to create imperfections in the mother materials by inserting impurities in certain amounts using certain methods. Doping of TiO₂ to reduce bandgap had an early success using nitrogen as a dopant source [23]. Since then, there was an extensive study on metal and non-metal doping of TiO₂. Niobium doped TiO₂ attracted massive attention especially in photocatalysis and dye-sensitized solar cells as an anode material. After doping, the Nb element can provide excess electrons in TiO₂ conduction band. The increase of electron concentration makes the electron conductivity improved due to the positive shift of conduction band minimum (CBM) [24]. For solar cells application or self-powered photodetector, this can help suppressing recombination in TiO₂/electrolyte interface. Nb doping on TiO₂ can also help in lowering the bandgap to extend the absorption of TiO₂ into the visible region and thus making it a visible light active catalyst under solar irradiation [25].

Other than metal doping, non-metal doping such as B, C, and N has also been extensively studied during the past years. B-doped TiO₂ has been proven to enhance the performance of solar cells [26]. This increase was mainly due to the improvement of the TiO₂ in its mobility and crystallinity. High crystallinity of B-doped TiO₂ comes from the B atom that is present in the TiO₂ matrix as a nucleus due to B³⁺ having smaller ionic radius (20 pm) than Ti⁴⁺ (60.5 pm), providing a good crystal growth. As for mobility, the TiO₂ nanorods crystalline structure was improved as the boron atom partially reduce the Ti⁴⁺. Recently, co-doping of both metal and non-metal ions has been attracting attention to enhance its functional properties in a single deposition. For instances, a past research has shown successful co-doping of Nb and N as metal and non-metal element, respectively [27]. By using these two materials, the material was reported to have increased photocatalytic activity from N doping and conductivity from

REFERENCES

- [1] T. Koutchma, "Basic Principles of UV Light Generation," in *Food Plant Safety*, First., Elsevier, 2014, pp. 3–13.
- [2] M. Addamo, M. Bellardita, A. Di Paola, and L. Palmisano, "Preparation and photoactivity of nanostructured anatase, rutile and brookite TiO₂ thin films.," *Chem. Commun. (Camb).*, no. 47, pp. 4943–4945, 2006, doi: 10.1039/b612172a.
- [3] Y. Liao, W. Que, Q. Jia, Y. He, J. Zhang, and P. Zhong, "Controllable synthesis of brookite/anatase/rutile TiO₂ nanocomposites and single-crystalline rutile nanorods array," *J. Mater. Chem.*, vol. 22, no. 16, pp. 7937–7944, 2012, doi: 10.1039/c2jm16628c.
- [4] E. N. Bunting, "Phase equilibria in the systems TiO₂, TiO₂-SiO₂ and TiO₂-Al₂O₃," *Bur. Stand. J. Res.*, vol. 11, no. November, 1933, doi: 10.6028/jres.011.049.
- [5] W. Y. C. S D Mo, "Electronic and optical properties of titanium dioxide: rutile, anatase and brookite," *Phys. Rev. B*, vol. 51, no. 19, pp. 50–59, 1995, doi: 10.1103/PhysRevB.51.13023.
- [6] J. Zhang, P. Zhou, J. Liu, and J. Yu, "New understanding of the difference of photocatalytic activity among anatase, rutile and brookite TiO₂," *Phys. Chem. Chem. Phys.*, vol. 16, no. 38, pp. 20382–20386, 2014, doi: 10.1039/C4CP02201G.
- [7] H. Yang, S. Zhu, and N. Pan, "Studying the mechanisms of titanium dioxide as ultraviolet-blocking additive for films and fabrics by an improved scheme," *J. Appl. Polym. Sci.*, vol. 92, no. 5, pp. 3201–3210, 2004, doi: 10.1002/app.20327.
- [8] Y. Li, X. Lv, and J. Li, "High performance binderless TiO₂ nanowire arrays electrode for lithium-ion battery," *Appl. Phys. Lett.*, vol. 95, no. 11, pp. 2009–2011, 2009, doi: 10.1063/1.3224888.

- [9] X. D. Tang *et al.*, “Study of Nd³⁺, Pd²⁺, Pt⁴⁺, and Fe³⁺ dopant effect on photoreactivity of TiO₂ nanoparticles,” *J. Biochem.*, vol. 99, no. 10, 2002.
- [10] X. Chen and S. S. Mao, “Titanium Dioxide Nanomaterials : Synthesis , Properties , Modifications , and Applications,” *Chem. Rev.*, vol. 107, pp. 2891–2959, 2007.
- [11] E. Comini, C. Baratto, G. Faglia, M. Ferroni, A. Vomiero, and G. Sberveglieri, “Quasi-one dimensional metal oxide semiconductors: Preparation, characterization and application as chemical sensors,” *Prog. Mater. Sci.*, vol. 54, no. 1, pp. 1–67, 2009, doi: 10.1016/j.pmatsci.2008.06.003.
- [12] S. S. Mali *et al.*, “Hydrothermal synthesis of rutile TiO₂ nanoflowers using Brønsted Acidic Ionic Liquid [BAIL]: Synthesis, characterization and growth mechanism,” *CrystEngComm*, vol. 14, no. 6, p. 1920, 2012, doi: 10.1039/c2ce06476f.
- [13] Y. X. Zhang, G. H. Li, Y. X. Jin, Y. Zhang, J. Zhang, and L. D. Zhang, “Hydrothermal synthesis and photoluminescence of TiO₂ nanowires,” vol. 365, pp. 300–304, 2002.
- [14] P. Dong, Y. Wang, B. Liu, L. Guo, Y. Huang, and S. Yin, “Applied Surface Science Effect of hydrothermal reaction time on morphology and photocatalytic activity of H₂Ti₃O₇ nanotubes obtained via a rapid synthesis route,” *Appl. Surf. Sci.*, vol. 258, no. 18, pp. 7052–7058, 2012, doi: 10.1016/j.apsusc.2012.03.164.
- [15] J. G. Lu, P. Chang, and Z. Fan, “Quasi-one-dimensional metal oxide materials- Synthesis, properties and applications,” *Mater. Sci. Eng. R Reports*, vol. 52, no. 1–3, pp. 49–91, 2006, doi: 10.1016/j.mser.2006.04.002.
- [16] P. Dong, Y. Wang, B. Liu, L. Guo, Y. Huang, and S. Yin, “Effect of hydrothermal reaction time on morphology and photocatalytic activity of H₂Ti₃O₇ nanotubes obtained via a rapid synthesis route,” *Appl. Surf. Sci.*, vol. 258, no. 18, pp. 7052–7058, 2012, doi: 10.1016/j.apsusc.2012.03.164.
- [17] A. C. Arias, J. D. MacKenzie, I. McCulloch, J. Rivnay, and A. Salleo, “Materials and applications for large area electronics: Solution-based approaches,” *Chem. Rev.*, vol. 110, no. 1, pp. 3–24, 2010, doi: 10.1021/cr900150b.
- [18] L. Forro *et al.*, “High mobility n-type charge carriers in large single crystals,” *New York*, vol. 75, pp. 633–635, 1994.
- [19] S. U. M. Khan, M. Al-Shahry, and W. B. Ingler, “Efficient photochemical water splitting by a chemically modified n-TiO₂,” *Science (80-.)*, vol. 297, no. 5590, pp. 2243–2245,

- 2002, doi: 10.1126/science.1075035.
- [20] C. Zhang, Y. Jia, Y. Jing, Y. Yao, J. Ma, and J. Sun, "Effect of non-metal elements (B, C, N, F, P, S) mono-doping as anions on electronic structure of SrTiO₃," *Comput. Mater. Sci.*, vol. 79, pp. 69–74, 2013, doi: 10.1016/j.commatsci.2013.06.009.
- [21] S. In *et al.*, "Effective Visible Light-Activated B-Doped and B, N-Codoped TiO₂ Photocatalysts," *J. Am. Chem. Soc.*, vol. 129, pp. 13790–13791, 2007, doi: 10.1021/ja0749237.
- [22] M. S. H. Al-Furjan, K. Cheng, and W. Weng, "Influences of mg doping on the electrochemical performance of TiO₂ nanodots based biosensor electrodes," *Adv. Mater. Sci. Eng.*, vol. 2014, 2014, doi: 10.1155/2014/965821.
- [23] R. Asahi, T. Morikawa, T. Ohwaki, K. Aoki, and Y. Taga, "Visible-light photocatalysis in nitrogen-doped titanium oxides," *Science (80-.)*, vol. 293, no. 5528, pp. 269–271, 2001, doi: 10.1126/science.1061051.
- [24] H. Su *et al.*, "Electrochimica Acta The Synthesis of Nb-doped TiO₂ Nanoparticles for Improved-Performance Dye Sensitized Solar Cells," *Electrochim. Acta*, vol. 182, pp. 230–237, 2015, doi: 10.1016/j.electacta.2015.09.072.
- [25] D. Y. Lee, J. H. Park, Y. H. Kim, M. H. Lee, and N. I. Cho, "Effect of Nb doping on morphology, crystal structure, optical band gap energy of TiO₂ thin films," *Curr. Appl. Phys.*, vol. 14, no. 3, pp. 421–427, 2014, doi: 10.1016/j.cap.2013.12.025.
- [26] Y. C. Tu, H. Lim, C. Y. Chang, J. J. Shyue, and W. F. Su, "Enhancing performance of P3HT: TiO₂ solar cells using doped and surface modified TiO₂ nanorods," *J. Colloid Interface Sci.*, vol. 448, pp. 315–319, 2015, doi: 10.1016/j.jcis.2015.02.015.
- [27] N. P. Chadwick, E. N. K. Glover, S. Sathasivam, and S. N. Basahel, "Photo-activity and Low Resistivity in N/Nb Co-doped TiO₂ Thin Films by Combinatorial AACVD," *J. Mater. Chem. A*, vol. 4, no. 2, pp. 407–415, 2016.
- [28] H. Wang and J. P. Lewis, "Second-generation photocatalytic materials: Anion-doped TiO₂," *J. Phys. Condens. Matter*, vol. 18, no. 2, pp. 421–434, 2006, doi: 10.1088/0953-8984/18/2/006.
- [29] M. Duta *et al.*, "Nb-doped TiO₂ sol-gel films for CO sensing applications," *Mater. Sci. Semicond. Process.*, vol. 42, pp. 397–404, 2016, doi: 10.1016/j.mssp.2015.11.004.

- [30] G. Peng *et al.*, “UV-induced SiC nanowire sensors,” *J. Phys. D. Appl. Phys.*, vol. 48, no. 5, p. 055102, 2015, doi: 10.1088/0022-3727/48/5/055102.
- [31] Z. Jakšić, M. Maksimović, and M. Sarajlić, “Silver–silica transparent metal structures as bandpass filters for the ultraviolet range,” *J. Opt. A Pure Appl. Opt.*, vol. 7, no. 1, pp. 51–55, 2004, doi: 10.1088/1464-4258/7/1/008.
- [32] E. Roduner, “Size matters: why nanomaterials are different,” *Chem. Soc. Rev.*, vol. 35, no. 7, p. 583, 2006, doi: 10.1039/b502142c.
- [33] M. Valden, “Onset of Catalytic Activity of Gold Clusters on Titania with the Appearance of Nonmetallic Properties,” *Science (80-.)*, vol. 281, no. 5383, pp. 1647–1650, 1998, doi: 10.1126/science.281.5383.1647.
- [34] P. Soundarrajan, K. Sankarasubramanian, T. Logu, K. Sethuraman, and K. Ramamurthi, “Growth of rutile TiO₂ nanorods on TiO₂ seed layer prepared using facile low cost chemical methods,” *Mater. Lett.*, vol. 116, pp. 191–194, Feb. 2014, doi: 10.1016/j.matlet.2013.11.026.
- [35] J. H. Kim, T. K. Yun, J. Y. Bae, and K. S. Ahn, “Enhanced carrier transport of N-doped TiO₂ for photoelectrochemical cells,” *Jpn. J. Appl. Phys.*, vol. 48, no. 12, 2009, doi: 10.1143/JJAP.48.120204.
- [36] A. Fujishima and K. Honda, “© 1972 Nature Publishing Group,” *Nature*, vol. 238, pp. 37–38, 1972.
- [37] A. P. Popov, A. V. Priezzhev, J. Lademann, and R. Myllylä, “TiO₂ nanoparticles as an effective UV-B radiation skin-protective compound in sunscreens,” *J. Phys. D. Appl. Phys.*, vol. 38, no. 15, pp. 2564–2570, 2005, doi: 10.1088/0022-3727/38/15/006.
- [38] A. J. Haider, R. H. AL–Anbari, G. R. Kadhim, and C. T. Salame, “Exploring potential Environmental applications of TiO₂ Nanoparticles,” *Energy Procedia*, vol. 119, pp. 332–345, 2017, doi: 10.1016/j.egypro.2017.07.117.
- [39] B. A. van Driel, P. J. Kooyman, K. J. van den Berg, A. Schmidt-Ott, and J. Dik, “A quick assessment of the photocatalytic activity of TiO₂ pigments - From lab to conservation studio!,” *Microchem. J.*, vol. 126, pp. 162–171, 2016, doi: 10.1016/j.microc.2015.11.048.
- [40] Z. Liu, X. Su, G. Hou, S. Bi, Z. Xiao, and H. Jia, “Spherical TiO₂ aggregates with different building units for dye-sensitized solar cells,” *Nanoscale*, vol. 5, no. 17, pp.

- 8177–83, 2013, doi: 10.1039/c3nr01767b.
- [41] K. Lee, A. Mazare, and P. Schmuki, “One-dimensional titanium dioxide nanomaterials: Nanotubes,” *Chem. Rev.*, vol. 114, no. 19, 2014, doi: 10.1021/cr500061m.
- [42] G. E. Patil, D. D. Kajale, V. B. Gaikwad, and G. H. Jain, “Spray Pyrolysis Deposition of Nanostructured Tin Oxide Thin Films,” *ISRN Nanotechnol.*, vol. 2012, pp. 1–5, 2012, doi: 10.5402/2012/275872.
- [43] A. Ranga Rao and V. Dutta, “Low-temperature synthesis of TiO₂ nanoparticles and preparation of TiO₂ thin films by spray deposition,” *Sol. Energy Mater. Sol. Cells*, vol. 91, no. 12, pp. 1075–1080, 2007, doi: 10.1016/j.solmat.2007.03.001.
- [44] G. El Fidha *et al.*, “Physical and photocatalytic properties of sprayed Dy doped ZnO thin films under sunlight irradiation for degrading methylene blue,” *RSC Adv.*, vol. 11, no. 40, pp. 24917–24925, 2021, doi: 10.1039/d1ra03967a.
- [45] X. Wang and J. Shi, “Evolution of titanium dioxide one-dimensional nanostructures from surface-reaction-limited pulsed chemical vapor deposition,” *J. Mater. Res.*, vol. 28, no. 3, pp. 270–279, 2013, doi: 10.1557/jmr.2012.356.
- [46] C.-W. Wang, J.-B. Chen, L.-Q. Wang, Y.-M. Kang, D.-S. Li, and F. Zhou, “Single crystal TiO₂ nanorods: Large-scale synthesis and field emission,” *Thin Solid Films*, vol. 520, no. 15, pp. 5036–5041, 2012, doi: 10.1016/j.tsf.2012.03.039.
- [47] D.-S. Li *et al.*, “Aligned rutile TiO₂ nanorods: Facile synthesis and field emission,” *Superlattices Microstruct.*, vol. 59, pp. 187–195, 2013, doi: 10.1016/j.spmi.2013.04.010.
- [48] P. Kajitvichyanukul, J. Ananpattarachai, and S. Pongpom, “Sol-gel preparation and properties study of TiO₂ thin film for photocatalytic reduction of chromium(VI) in photocatalysis process,” *Sci. Technol. Adv. Mater.*, vol. 6, no. 3-4 SPEC. ISS., pp. 352–358, 2005, doi: 10.1016/j.stam.2005.02.014.
- [49] Ming Zhang, Y. Bando, and K. Wada, “Sol-gel template preparation of TiO₂ nanotubes and nanorods,” *J. Mater. Sci. Lett.*, vol. 20, no. 2, pp. 167–170, 2001, doi: 10.1023/A:1006739713220.
- [50] N. Venkatachalam, M. Palanichamy, and V. Murugesan, “Sol-gel preparation and characterization of nanosize TiO₂: Its photocatalytic performance,” *Mater. Chem. Phys.*, vol. 104, no. 2–3, pp. 454–459, 2007, doi: 10.1016/j.matchemphys.2007.04.003.

- [51] S. J. Limmer, T. P. Chou, and G. Z. Cao, "A study on the growth of TiO₂ nanorods using sol electrophoresis," *J. Mater. Sci. Mater. Electron.*, vol. 9, no. 39, pp. 895–901, 2004.
- [52] D. Bokov *et al.*, "Nanomaterial by Sol-Gel Method: Synthesis and Application," *Adv. Mater. Sci. Eng.*, vol. 2021, 2021, doi: 10.1155/2021/5102014.
- [53] M. Sivakumar and A. Muthupandian, *Cavitation- A Novel Energy-Efficient Technique for the Generation of Nanomaterials*. 2014.
- [54] J. H. Bang and K. S. Suslick, "Applications of ultrasound to the synthesis of nanostructured materials," *Adv. Mater.*, vol. 22, no. 10, pp. 1039–1059, 2010, doi: 10.1002/adma.200904093.
- [55] M. Kumar, R. S. Bishnoi, A. K. Shukla, and C. P. Jain, "Techniques for formulation of nanoemulsion drug delivery system: A review," *Prev. Nutr. Food Sci.*, vol. 24, no. 3, pp. 225–234, 2019, doi: 10.3746/pnf.2019.24.3.225.
- [56] A. Hassanjani-Roshan, S. M. Kazemzadeh, M. R. Vaezi, and A. Shokuhfar, "The effect of sonication power on the sonochemical synthesis of titania nanoparticles," *J. Ceram. Process. Res.*, vol. 12, no. 3, pp. 299–303, 2011.
- [57] N. Wongpisutpaisan and C. Kahattha, "Titanium Dioxide Nanostructures Synthesized by Sonochemical – hydrothermal Process," *J. Met. Mater. Miner.*, vol. 23, no. 1, pp. 19–24, 2013.
- [58] K. Fujihara, A. Kumar, R. Jose, S. Ramakrishna, and S. Uchida, "Spray deposition of electrospun TiO₂ nanorods for dye-sensitized solar cell," *Nanotechnology*, vol. 18, no. 365709, pp. 1–6, 2007, doi: 10.1088/0957-4484/18/36/365709.
- [59] H. Zhang *et al.*, "Fabrication of highly ordered TiO₂ nanorod/nanotube adjacent arrays for photoelectrochemical applications," *Langmuir*, vol. 26, no. 13, pp. 11226–11232, 2010, doi: 10.1021/la1005314.
- [60] A. M. Selman and Z. Hassan, "Highly sensitive fast-response UV photodiode fabricated from rutile TiO₂ nanorod array on silicon substrate," *Sensors Actuators A Phys.*, vol. 221, pp. 15–21, Jan. 2015, doi: 10.1016/j.sna.2014.10.041.
- [61] Y. Wang, L. Zhang, K. Deng, X. Chen, and Z. Zou, "Low Temperature Synthesis and Photocatalytic Activity of Rutile TiO₂ Nanorod Superstructures," *J. Phys. Chem. C*, vol. 111, pp. 2709–2714, 2007, doi: 10.1021/jp066519k.

- [62] S. Venkatachalam, H. Hayashi, T. Ebina, and H. Nanjo, "Preparation and Characterization of Nanostructured TiO₂ Thin Films by Hydrothermal and Anodization Methods," *Optoelectron. - Adv. Mater. Devices*, pp. 115–136, 2013, doi: 10.5772/51254.
- [63] L. Dong *et al.*, "Hydrothermal growth of rutile TiO₂ nanorod films on titanium substrates," *Thin Solid Films*, vol. 519, no. 15, pp. 4634–4640, May 2011, doi: 10.1016/j.tsf.2011.01.008.
- [64] Y. Li, M. Guo, M. Zhang, and X. Wang, "Hydrothermal synthesis and characterization of TiO₂ nanorod arrays on glass substrates," *Mater. Res. Bull.*, vol. 44, no. 6, pp. 1232–1237, 2009, doi: 10.1016/j.materresbull.2009.01.009.
- [65] J. J. Yuan, H. D. Li, S. Y. Gao, D. D. Sang, L. a. Li, and D. Lu, "Hydrothermal synthesis, characterization and properties of TiO₂ nanorods on boron-doped diamond film," *Mater. Lett.*, vol. 64, no. 18, pp. 2012–2015, 2010, doi: 10.1016/j.matlet.2010.06.033.
- [66] H.-E. Wang *et al.*, "Hydrothermal synthesis of ordered single-crystalline rutile TiO₂ nanorod arrays on different substrates," *Appl. Phys. Lett.*, vol. 96, no. 26, p. 263104, 2010, doi: 10.1063/1.3442913.
- [67] M. N. Tahir *et al.*, "Facile Synthesis and Characterization of Functionalized, Monocrystalline Rutile TiO₂ Nanorods," *Am. Chem. Soc.*, no. 21, pp. 5209–5212, 2006.
- [68] S. P. Chang, R. W. Chuang, S. J. Chang, C. Y. Lu, Y. Z. Chiou, and S. F. Hsieh, "Surface HCl treatment in ZnO photoconductive sensors," *Thin Solid Films*, vol. 517, no. 17, pp. 5050–5053, 2009, doi: 10.1016/j.tsf.2009.03.042.
- [69] C. Soci, A. Zhang, X.-Y. Bao, H. Kim, Y. Lo, and D. Wang, "Nanowire Photodetectors," *J. Nanosci. Nanotechnol.*, vol. 10, no. 3, pp. 1430–1449, 2010, doi: 10.1166/jnn.2010.2157.
- [70] D. Caputo, G. de Cesare, A. Nascetti, and M. Tucci, "Innovative window layer for amorphous silicon/amorphous silicon carbide UV sensor," *J. Non. Cryst. Solids*, vol. 352, no. 9-20 SPEC. ISS., pp. 1818–1821, 2006, doi: 10.1016/j.jnoncrysol.2005.09.052.
- [71] J. D. Hwang and C. C. Lin, "Gallium nitride photoconductive ultraviolet sensor with a sputtered transparent indium-tin-oxide ohmic contact," *Thin Solid Films*, vol. 491, no. 1–2, pp. 276–279, 2005, doi: 10.1016/j.tsf.2005.05.044.
- [72] K. Hayashi *et al.*, "Temporal response of UV sensors made of highly oriented diamond films by 193 and 313 nm laser pulses," *Diam. Relat. Mater.*, vol. 10, no. 9–10, pp. 1794–

- 1798, 2001, doi: 10.1016/S0925-9635(01)00451-4.
- [73] C. J. Lee, C. H. Won, J. H. Lee, S. H. Hahm, and H. Park, "Selectively enhanced uv-a photoresponsivity of a gan msm uv photodetector with a step-graded alxgal-xn buffer layer," *Sensors (Switzerland)*, vol. 17, no. 7, pp. 1–9, 2017, doi: 10.3390/s17071684.
- [74] A. Kusior, J. Banas, A. Trenczek-Zajac, P. Zubrzycka, A. Micek-Ilnicka, and M. Radecka, "Structural properties of TiO₂nanomaterials," *J. Mol. Struct.*, vol. 1157, pp. 327–336, 2018, doi: 10.1016/j.molstruc.2017.12.064.
- [75] Z. Sun, T. Liao, L. Sheng, L. Kou, J. H. Kim, and S. X. Dou, "Deliberate Design of TiO₂ Nanostructures towards Superior Photovoltaic Cells," *Chem. - A Eur. J.*, no. May, pp. 11357–11364, 2016, doi: 10.1002/chem.201601546.
- [76] Q. Li, R. Liu, B. Zou, T. Cui, and B. Liu, "Effects of hydrothermal conditions on the morphology and phase composition of synthesized TiO₂ nanostructures," *Phys. B Phys. Condens. Matter*, vol. 445, pp. 42–47, 2014, doi: 10.1016/j.physb.2014.03.079.
- [77] U. M. Nayef, K. A. Hubeatir, and Z. J. Abdulkareem, "Ultraviolet photodetector based on TiO₂nanoparticles/porous silicon hetrojunction," *Optik (Stuttg.)*, vol. 127, no. 5, pp. 2806–2810, 2016, doi: 10.1016/j.ijleo.2015.12.002.
- [78] H. Wang *et al.*, "A high-sensitive ultraviolet photodetector composed of double-layered TiO₂nanostucture and Au nanoparticles film based on Schottky junction," *Mater. Chem. Phys.*, vol. 194, pp. 42–48, 2017, doi: 10.1016/j.matchemphys.2017.03.019.
- [79] N. H. Kargan, M. Aliahmad, and S. Azizi, "Detecting Ultra-Violet Radiation by Using Titanium Dioxide Nanoparticles," *Soft Nanosci. Lett.*, vol. 02, no. 03, pp. 29–33, 2012, doi: 10.4236/snsl.2012.23006.
- [80] C. D. Wenji Zheng Xiangcun Li, Gaohong He, Xiaoming Yan, Rui Zhao, "RSC Advances," *RSC Adv.*, no. 41, pp. 21340–21346, 2014.
- [81] Y. Xie *et al.*, "High-performance self-powered UV photodetectors based on TiO₂ nano-branched arrays," *Nanotechnology*, vol. 25, no. 7, 2014, doi: 10.1088/0957-4484/25/7/075202.
- [82] M. Zhang, D. Li, J. Zhou, W. Chen, and S. Ruan, "Ultraviolet detector based on TiO₂nanowire array-polymer hybrids with low dark current," *J. Alloys Compd.*, vol. 618, pp. 233–235, 2015, doi: 10.1016/j.jallcom.2014.07.040.

- [83] G. Liu *et al.*, “Effects of growth substrates on the morphologies of TiO₂nanowire arrays and the performance of assembled UV detectors,” *Appl. Surf. Sci.*, vol. 315, no. 1, pp. 55–58, 2014, doi: 10.1016/j.apsusc.2014.07.115.
- [84] A. Zaleska, “Doped-TiO₂: A Review,” *Recent Patents Eng.*, vol. 2, no. 3, pp. 157–164, 2008, doi: 10.2174/187221208786306289.
- [85] S. Sato, “Photocatalytic activity of NO_x-doped TiO₂ in the visible light region,” *Chem. Phys. Lett.*, vol. 123, no. 1–2, pp. 126–128, 1986, doi: 10.1016/0009-2614(86)87026-9.
- [86] Y. C. Zhang, M. Yang, G. Zhang, and D. D. Dionysiou, “HNO₃-involved one-step low temperature solvothermal synthesis of N-doped TiO₂ nanocrystals for efficient photocatalytic reduction of Cr(VI) in water,” *Appl. Catal. B Environ.*, vol. 142–143, pp. 249–258, 2013, doi: 10.1016/j.apcatb.2013.05.023.
- [87] A. M. Czoska *et al.*, “The nature of defects in fluorine-doped TiO₂,” *J. Phys. Chem. C*, vol. 112, no. 24, pp. 8951–8956, 2008, doi: 10.1021/jp8004184.
- [88] S. C. Padmanabhan *et al.*, “A simple sol - Gel processing for the development of high-temperature stable photoactive anatase titania,” *Chem. Mater.*, vol. 19, no. 18, pp. 4474–4481, 2007, doi: 10.1021/cm070980n.
- [89] P. Periyat, D. E. McCormack, S. J. Hinder, and S. C. Pillai, “One-pot synthesis of anionic (nitrogen) and cationic (sulfur) codoped high-temperature stable, visible light active, anatase Photocatalysts,” *J. Phys. Chem. C*, vol. 113, no. 8, pp. 3246–3253, 2009, doi: 10.1021/jp808444y.
- [90] M. B. Sarkar *et al.*, “Improved UV Photodetection by Indium Doped TiO₂ Thin Film Based Photodetector,” *J. Nanosci. Nanotechnol.*, vol. 18, no. 7, pp. 4898–4903, 2017, doi: 10.1166/jnn.2018.15295.
- [91] N. Prakash *et al.*, “Effect of Erbium on the Photocatalytic Activity of TiO₂/Ag Nanocomposites under Visible Light Irradiation,” *ChemPhysChem*, vol. 16, no. 14, pp. 3084–3092, 2015, doi: 10.1002/cphc.201500492.
- [92] Y. X. Dong, X. L. Wang, E. M. Jin, S. M. Jeong, B. Jin, and S. H. Lee, “One-step hydrothermal synthesis of Ag decorated TiO₂ nanoparticles for dye-sensitized solar cell application,” *Renew. Energy*, vol. 135, pp. 1207–1212, 2019, doi: 10.1016/j.renene.2018.12.062.
- [93] H. Li *et al.*, “Surface plasmon resonance-enhanced solar-driven photocatalytic

- performance from Ag nanoparticle-decorated self-floating porous black TiO₂ foams,” *Appl. Catal. B Environ.*, vol. 220, pp. 111–117, 2018, doi: 10.1016/j.apcatb.2017.08.023.
- [94] Y. Cong, J. Zhang, F. Chen, and M. Anpo, “Synthesis and characterization of nitrogen-doped TiO₂ nanophotocatalyst with high visible light activity,” *J. Phys. Chem. C*, vol. 111, no. 19, pp. 6976–6982, 2007, doi: 10.1021/jp0685030.
- [95] X. Mou, J. Wu, D. Zhang, and L. Zhang, “Improved-Performance Dye-Sensitized Solar Cells Using Nb-Doped TiO₂ Electrodes : Efficient Electron Injection and Transfer,” pp. 509–515, 2010, doi: 10.1002/adfm.200901292.
- [96] M. Yang *et al.*, “Improved charge transport of Nb-doped TiO₂nanorods in methylammonium lead iodide bromide perovskite solar cells,” *J. Mater. Chem. A*, vol. 2, no. 46, pp. 19616–19622, 2014, doi: 10.1039/c4ta02635g.
- [97] Y. Liu, P. Wang, C. Wang, and Y. Ao, “Polymeric carbon nitride coated Nb-TiO₂ nanorod arrays with enhanced photoelectrocatalytic activity under visible light irradiation,” *Inorg. Chem. Commun.*, vol. 101, no. November 2018, pp. 113–116, 2019, doi: 10.1016/j.inoche.2018.12.017.
- [98] K. C. Ok *et al.*, “Semiconducting behavior of niobium-doped titanium oxide in the amorphous state,” *Appl. Phys. Lett.*, vol. 100, no. 14, 2012, doi: 10.1063/1.3698389.
- [99] H. Y. Wang, H. Yang, L. Zhang, J. Chen, and B. Liu, “Niobium Doping Enhances Charge Transport in TiO₂Nanorods,” *ChemNanoMat*, vol. 2, no. 7, pp. 660–664, 2016, doi: 10.1002/cnma.201600035.
- [100] J. Xu, Y. Ao, M. Chen, and D. Fu, “Low-temperature preparation of Boron-doped titania by hydrothermal method and its photocatalytic activity,” *J. Alloys Compd.*, vol. 484, no. 1–2, pp. 73–79, 2009, doi: 10.1016/j.jallcom.2009.04.156.
- [101] J. Zheng, Z. Liu, X. Liu, X. Yan, D. Li, and W. Chu, “Facile hydrothermal synthesis and characteristics of B-doped TiO₂ hybrid hollow microspheres with higher photocatalytic activity,” *J. Alloys Compd.*, vol. 509, no. 9, pp. 3771–3776, 2011, doi: 10.1016/j.jallcom.2010.12.152.
- [102] Y. C. Tu, J. F. Lin, W. C. Lin, C. P. Liu, J. J. Shyue, and W. F. Su, “Improving the electron mobility of TiO₂ nanorods for enhanced efficiency of a polymer-nanoparticle solar cell,” *CrystEngComm*, vol. 14, no. 14, pp. 4772–4776, 2012, doi:

- 10.1039/c2ce25489a.
- [103] Y. Wang *et al.*, “Boron-Doped TiO₂ for Efficient Electrocatalytic N₂ Fixation to NH₃ at Ambient Conditions,” *ACS Sustain. Chem. Eng.*, vol. 7, no. 1, pp. 117–122, 2019, doi: 10.1021/acssuschemeng.8b05332.
- [104] W. Q. Wu *et al.*, “Hydrothermal fabrication of hierarchically anatase TiO₂ nanowire arrays on FTO glass for dye-sensitized solar cells,” *Sci. Rep.*, vol. 3, pp. 1–7, 2013, doi: 10.1038/srep01352.
- [105] B. Liu and E. S. Aydil, “Growth of Oriented Single-Crystalline Rutile TiO Nanorods on Transparent Conducting Substrates for Dye-Sensitized Solar Cells Growth of Oriented Single-Crystalline Rutile TiO₂ Nanorods on Transparent Conducting Substrates for Dye-Sensitized Solar Cells,” *Glass*, no. 9, pp. 3985–3990, 2009, doi: 10.1021/ja8078972.
- [106] S. Yang, L. Gao, and S. Microstructure, “Fabrication and Characterization of Nanostructurally Flowerlike Aggregates of TiO₂ via a Surfactant-free Solution Route : Effect of Various Reaction Media,” vol. 34, no. 7, pp. 1044–1045, 2005, doi: 10.1246/cl.2005.1044.
- [107] S. Yang, L. Gao, and S. Microstructure, “Low-temperature Synthesis of Crystalline TiO₂ Nanorods : Mass Production Assisted by Surfactant,” vol. 34, no. 7, pp. 964–965, 2005, doi: 10.1246/cl.2005.964.
- [108] X. Ji, W. Liu, Y. Leng, and A. Wang, “Facile Synthesis of ZnO@TiO₂ Core-Shell Nanorod Thin Films for Dye-Sensitized Solar Cells,” *J. Nanomater.*, vol. 2015, pp. 1–5, 2015, doi: 10.1155/2015/647089.
- [109] W. Guo *et al.*, “Rectangular bunched rutile TiO₂ nanorod arrays grown on carbon fiber for dye-sensitized solar cells.,” *J. Am. Chem. Soc.*, vol. 134, no. 9, pp. 4437–41, 2012, doi: 10.1021/ja2120585.
- [110] T.-D. Nguyen Phan, H.-D. Pham, T. Viet Cuong, E. Jung Kim, S. Kim, and E. Woo Shin, “A simple hydrothermal preparation of TiO₂ nanomaterials using concentrated hydrochloric acid,” *J. Cryst. Growth*, vol. 312, no. 1, pp. 79–85, Dec. 2009, doi: 10.1016/j.jcrysgro.2009.09.032.
- [111] M. H. Mamat, “Fabrication and Characterisation of Aligned Zinc Oxide Nanorod Array-Based Ultraviolet Photoconductive Sensors,” Universiti Teknologi Mara, 2013.

- [112] X. Meng *et al.*, “Formation Mechanism of Rutile TiO₂ Rods on Fluorine Doped Tin Oxide Glass,” *J. Nanosci. Nanotechnol.*, vol. 14, no. 11, pp. 8839–8844, 2014, doi: 10.1166/jnn.2014.10016.
- [113] Y. Zhang, C. X. Harris, P. Wallenmeyer, J. Murowchick, and X. Chen, “Asymmetric lattice vibrational characteristics of rutile TiO₂ as revealed by laser power dependent raman spectroscopy,” *J. Phys. Chem. C*, vol. 117, no. 45, pp. 24015–24022, 2013, doi: 10.1021/jp406948e.
- [114] M. K. Ahmad *et al.*, “Raman investigation of rutile-phased TiO₂ nanorods/nanoflowers with various reaction times using one step hydrothermal method,” *J. Mater. Sci. Mater. Electron.*, vol. 27, no. 8, pp. 7920–7926, 2016, doi: 10.1007/s10854-016-4783-z.
- [115] J. S. Ko, N. Q. Le, D. R. Schlesinger, J. K. Johnson, and Z. Xia, “Novel niobium-doped titanium oxide towards electrochemical destruction of forever chemicals,” *Sci. Rep.*, vol. 11, no. 1, pp. 1–11, 2021, doi: 10.1038/s41598-021-97596-7.
- [116] S. Sugapriya, R. Sriram, and S. Lakshmi, “Effect of annealing on TiO₂ nanoparticles,” *Opt. - Int. J. Light Electron Opt.*, vol. 124, no. 21, pp. 4971–4975, Nov. 2013, doi: 10.1016/j.ijleo.2013.03.040.
- [117] M. Gotić *et al.*, “Raman investigation of nanosized TiO₂,” *J. Raman Spectrosc.*, vol. 28, no. 7, pp. 555–558, 1997, doi: 10.1002/(SICI)1097-4555(199707)28:7<555::AID-JRS118>3.0.CO;2-S.
- [118] G. Panchal, D. K. Shukla, R. J. Choudhary, V. R. Reddy, and D. M. Phase, “The effect of oxygen stoichiometry at the interface of epitaxial BaTiO₃/La_{0.7}Sr_{0.3}MnO₃ bilayers on its electronic and magnetic properties,” *J. Appl. Phys.*, vol. 122, no. 8, 2017, doi: 10.1063/1.5000133.
- [119] J.-S. Bae *et al.*, “Optical properties and Surface analysis of lithium incorporated Y₂O₃:Eu³⁺ ceramic phosphors,” *J. Anal. Sci. Technol.*, vol. 1, no. 2, pp. 92–97, 2010, doi: 10.5355/jast.2010.92.
- [120] Y. Yang, T. Sun, F. Ma, L. F. Huang, and Z. Zeng, “Superhydrophilic Fe³⁺-Doped TiO₂ films with long-lasting antifogging performance,” *ACS Appl. Mater. Interfaces*, vol. 13, no. 2, pp. 3377–3386, 2021, doi: 10.1021/acsami.0c18444.
- [121] S. A. Abdullah *et al.*, “Influence of substrate annealing on inducing Ti³⁺ and oxygen vacancy in TiO₂ thin films deposited via RF magnetron sputtering,” *Appl. Surf. Sci.*,

- vol. 462, no. August, pp. 575–582, 2018, doi: 10.1016/j.apsusc.2018.08.137.
- [122] Y. Liu, H. Ran, J. Fan, X. Zhang, J. Mao, and G. Shao, “Fabrication and photovoltaic performance of niobium doped TiO₂ hierarchical microspheres with exposed {001} facets and high specific surface area,” *Appl. Surf. Sci.*, vol. 410, pp. 241–248, 2017, doi: 10.1016/j.apsusc.2017.03.085.
- [123] J. Yue *et al.*, “Mesoporous niobium-doped titanium dioxide films from the assembly of crystalline nanoparticles: study on the relationship between the band structure, conductivity and charge storage mechanism,” *J. Mater. Chem. A*, vol. 5, no. 5, pp. 1978–1988, 2017, doi: 10.1039/c6ta06840e.
- [124] Y. Pang and P. Wynblatt, “Effects of Nb Doping and Segregation on the Grain Boundary Plane Distribution in TiO₂,” *J. Am. Ceram. Soc.*, vol. 671, no. 20723, pp. 666–671, 2006, doi: 10.1111/j.1551-2916.2005.00759.x.
- [125] K. M. Reddy, S. V. Manorama, and A. R. Reddy, “Bandgap studies on anatase titanium dioxide nanoparticles,” *Mater. Chem. Phys.*, no. 78, pp. 239–245, 2002.
- [126] M. Yang, B. Ding, and J. K. Lee, “Surface electrochemical properties of niobium-doped titanium dioxide nanorods and their effect on carrier collection efficiency of dye sensitized solar cells,” *J. Power Sources*, vol. 245, pp. 301–307, 2014, doi: 10.1016/j.jpowsour.2013.06.016.
- [127] L. Zheng *et al.*, “Novel D-A- π -a-type organic dyes containing a ladderlike dithienocyclopentacarbazole donor for effective dye-sensitized solar cells,” *ACS Omega*, vol. 2, no. 10, pp. 7048–7056, 2017, doi: 10.1021/acsomega.7b01387.
- [128] C. Huang, J. Bian, and R. Q. Zhang, “Role of Cl Ion Desorption in Photocurrent Enhancement of the Annealed Rutile Single-Crystalline TiO₂ Nanorod Arrays,” *J. Phys. Chem. C*, vol. 121, no. 34, pp. 18892–18899, 2017, doi: 10.1021/acs.jpcc.7b04071.
- [129] M. C. Mathpal, A. K. Tripathi, M. K. Singh, S. P. Gairola, S. N. Pandey, and A. Agarwal, “Effect of annealing temperature on Raman spectra of TiO₂ nanoparticles,” *Chem. Phys. Lett.*, vol. 555, pp. 182–186, 2013, doi: 10.1016/j.cplett.2012.10.082.
- [130] Y. Li, L. Wei, R. Zhang, Y. Chen, and J. Jiao, “Annealing effect on photovoltaic performance of CdSe quantum-dots- sensitized TiO₂ nanorod solar cells,” *J. Nanomater.*, vol. 2012, 2012, doi: 10.1155/2012/103417.
- [131] I. E. Grey, C. Li, C. M. MacRae, and L. A. Bursill, “Boron incorporation into rutile.

- Phase equilibria and structure considerations,” *J. Solid State Chem.*, vol. 127, no. 2, pp. 240–247, 1996, doi: 10.1006/jssc.1996.0380.
- [132] Q. Zhu *et al.*, “Microsphere assembly of rutile TiO₂ hierarchically hyperbranched nanorods: CdS sensitization and photovoltaic properties,” *Solid State Sci.*, vol. 13, no. 6, pp. 1299–1303, Jun. 2011, doi: 10.1016/j.solidstatesciences.2011.03.025.
- [133] J. Li, N. Lu, X. Quan, S. Chen, and H. Zhao, “Facile method for fabricating boron-doped TiO₂ nanotube array with enhanced photoelectrocatalytic properties,” *Ind. Eng. Chem. Res.*, vol. 47, no. 11, pp. 3804–3808, 2008, doi: 10.1021/ie0712028.
- [134] E. Finazzi, C. Di Valentin, and G. Pacchioni, “Boron-doped anatase TiO₂: Pure and hybrid DFT calculations,” *J. Phys. Chem. C*, vol. 113, no. 1, pp. 220–228, 2009, doi: 10.1021/jp8072238.
- [135] L. Li, F. Meng, X. Hu, L. Qiao, C. Q. Sun, and H. Tian, “TiO₂ Band Restructuring by B and P Dopants,” pp. 1–14, 2016, doi: 10.1371/journal.pone.0152726.
- [136] N. Feng *et al.*, “Unravelling the Efficient Photocatalytic Activity of Boron-induced Ti³⁺ Species in the Surface Layer of TiO₂,” *Sci. Rep.*, vol. 6, no. September, pp. 1–9, 2016, doi: 10.1038/srep34765.
- [137] B. Hu, Q. Zhang, L. Niu, J. Liu, J. Rao, and X. Zhou, “Microsphere assembly of boron-doped Rutile TiO₂ nanotubes with enhanced photoelectric performance,” *J. Mater. Sci. Mater. Electron.*, vol. 26, no. 11, pp. 8915–8921, 2015, doi: 10.1007/s10854-015-3573-3.
- [138] D. Zhao, Y. Yu, C. Cao, J. Wang, E. Wang, and Y. Cao, “The existing states of doped B³⁺ ions on the B doped TiO₂,” *Appl. Surf. Sci.*, vol. 345, pp. 67–71, 2015, doi: 10.1016/j.apsusc.2015.03.140.
- [139] B. Buchholz, E. Varga, T. Varga, K. Plank, J. Kiss, and Z. Kónya, “Structure and stability of boron doped titanate nanotubes and nanowires,” *Vacuum*, vol. 138, pp. 120–124, 2017, doi: 10.1016/j.vacuum.2016.11.038.
- [140] M. T. Aytekin, “Synthesis, characterization and photocatalytic activity of boron-doped titanium dioxide nanotubes,” vol. 1180, pp. 676–682, 2019, doi: 10.1016/j.molstruc.2018.12.056.
- [141] Y. Su, S. Han, X. Zhang, X. Chen, and L. Lei, “Preparation and visible-light-driven photoelectrocatalytic properties of boron-doped TiO₂ nanotubes,” vol. 110, pp. 239–

- 246, 2008, doi: 10.1016/j.matchemphys.2008.01.036.
- [142] S. Singh Surah, M. Vishwakarma, R. Kumar, R. Nain, S. Sirohi, and G. Kumar, “Tuning the electronic band alignment properties of TiO₂ nanotubes by boron doping,” *Results Phys.*, vol. 12, no. November 2018, pp. 1725–1731, 2019, doi: 10.1016/j.rinp.2019.01.081.
- [143] F. Paquin, J. Rivnay, A. Salleo, N. Stingelin, and C. Silva, “Multi-phase semicrystalline microstructures drive exciton dissociation in neat plastic semiconductors,” *J. Mater. Chem. C*, vol. 3, pp. 10715–10722, 2015, doi: 10.1039/b000000x.
- [144] S. W. Guo XY, Xu DP, Ding ZH, “Preparation and Raman Spectrum of Rutile Single Crystal Using Floating Zone Method,” *CHIN.PHYS.LETT.*, vol. 23, no. 6, p. 1645, 2006.



APPENDIX A

LIST OF PUBLICATIONS

1. S. M. Mokhtar, M.K. Ahmad, C.F. Soon, N.K.A. Hamed, and M. Shimomura, "Photovoltaic enhancement of nanostructured boron-doped rutile phase TiO₂ nanorods via facile hydrothermal method," *J Mater Sci: Mater Electron*, vol. 33, no. 12, pp. 9471-9482, 2022.
2. S. M. Mokhtar, M. K. Ahmad, S. Harish, N. K. A. Hamed, and M. Shimomura, "Surface chemistry and growth mechanism of highly oriented, single crystalline Nb-doped TiO₂ nanorods," *CrystEngComm*, vol. 22, no. 13, pp. 2380–2388, 2020.
3. S. M. Mokhtar, M. K. Ahmad, N. Nafarizal, C. F. Soon, M. H. Mamat, N. M. A. N. Ismail, A. S. Ameruddin, A. B. Suriani, M. Shimomura, K. Murakami., "High responsivity of ultraviolet sensor-based rutile-phased TiO₂ nanorod arrays using different bias voltage," *J. Aust. Ceram. Soc.*, vol. 56, no. 2, pp. 461–468, 2020.
4. S. M. Mokhtar, M.K. Ahmad, C.F. Soon, N. Nafarizal, A.B. Faridah, A.B. Suriani, M.H. Mamat, M. Shimomura, K. Murakami, "Fabrication and characterization of rutile-phased titanium dioxide (TiO₂) nanorods arrays with various reaction times using one step hydrothermal method," *Optik (Stuttg)*, vol. 154, pp. 510–515, 2018
5. N.K.A. Hamed, M.K Ahmad, N.H.H. Hairom, A.B. Faridah, M.H. Mamat, A. Mohamed, A.B. Suriani, N. Nafarizal, F.I.M Fazli, S.M Mokhtar, W.I.W Omar and M. Shimomura, "Dependence of photocatalysis on electron trapping in Ag-doped flowerlike rutile-phase TiO₂ film by facile hydrothermal method", *Applied Surface Science*, vol. 534, pp. 147571, 2020
6. M. K. Ahmad, S. M. Mokhtar, C. F. Soon, N. Nafarizal, A. B. Suriani, A. Mohamed, M. H. Mamat, M. F. Malek, M. Shimomura, and K. Murakami, "Raman investigation of rutile-phased TiO₂ nanorods/nanoflowers with various reaction times using one step hydrothermal method," *J. Mater. Sci. Mater. Electron*, 2016

LIST OF CONFERENCES PROCEEDING AND PRESENTATIONS

1. Salina Mohammad Mokhtar, Masaru Shimomura, Mohd Khairul Ahmad, Growth Study of Highly Oriented, Single-Crystalline Nb-doped TiO₂ Nanorods for Enhance Carrier Transport, Abstracts of Papers, 18th Japan Surface Vacuum Society Chubu Branch Academic Lecture, Nagoya, Japan, Dec. 2019



APPENDIX B

LIST OF AWARDS

1. Best paper award for 12th Malaysia Technical Universities Conference on Engineering and Technology, November 2021



PTTA UTHM
PERPUSTAKAAN TUNKU TUN AMINAH

APPENDIX C

VITA

Salina was born in Kuala Lumpur, Malaysia, on August 26, 1991. They attended elementary school in Sekolah Kebangsaan Labohan Dagang, and graduated from Sekolah Menengah Kebangsaan Banting in December 2008. Following April, they attended Kolej Matrikulasi Pulau Pinang as preparation before enrolling to Universiti Tun Hussein Onn Malaysia and received the degree of Bachelor of Electronic (Microelectronic) Engineering in August 2014. In April 2015, they started Master of Electrical Engineering from the same university and graduated in September 2017. They attended Shizuoka University in October 2017 and received Doctor of Engineering in Optical Electronics and Nanostructure Science in April 2021.



PTTA
PERPUSTAKAAN TUNKU TUN AMINAH